How did Jupiter form?

Calle Ahlgren

Lund Observatory
Lund University

2019-EXA141

Degree project of 15 higher education credits
February 2019

Supervisor: Anders Johansen

Lund Observatory
Box 43
SE-221 00 Lund
Sweden

Abstract

Two relatively new concepts in planetary science are planetary migration; wherein the planets migrate through the protoplanetary disk as they form, and pebble accretion; wherein the planetesimals which become terrestrial planets and giant planet cores grow through the accretion of small pebbles. Planetary migration has become a generally accepted concept but there is still much to be learned even about how it affected the formation of our own solar system. As such, the goal of this thesis is to add to this knowledge by investigating how far Jupiter might have migrated in the protoplanetary disk surrounding the young Sun.

This is done by performing simulations of the growth and migration of planets evolving in a protoplanetary disk. These simulations are carried out using different initial planetesimal parameters in terms of distance from the host star and starting time of the accretion in relation to the lifetime of the protoplanetary disk. The `Python` code developed for the thesis to perform the simulations does so by numerically integrating the mass and radial distance from the host star of evolving planets according to the Euler method. In the case of the planet mass the integration follows pebble accretion and subsequently gas accretion for such planets that grow massive enough. The integration of the radial distance from the host star follows recent solutions wherein the migration of a gas accreting planet is not tied to the gas accretion rate onto the star as has been previously suggested.

From the results of the simulations I find that the migration distance is heavily dependent on the ratio between the gas accretion and pebble accretion rates onto the host star. When using the low value of 0.01 for this ratio in the simulations Jupiter analogues are found to migrate almost 50 AU. By increasing the value to 0.1 on the other hand I find that the migration distance is reduced to less than 10 AU. The simulations in the thesis follow a simplified model of the planet formation process. As such, these results should be seen as a stepping stone towards more accurate results.

Acknowledgements

First off I want to thank my fiancee Louise for putting up with all my long hours stuck in front of the computer screen. I also want to thank what I will just call my Christmas day friends (so that I do not forget any names) for some great support and interest in my thesis. Finally I want to thank my supervisor Anders Johansen for answering and having patience with all my incessant questions as well as for his advice during the writing process.

Populärvetenskaplig beskrivning

Vet du hur planeterna i vårt solsystem kom att kretsa på sina nuvarande avstånd från solen? Inte? Var inte orolig, det vet inte jag heller och inte ens astronomer som studerar planetformation vet riktigt säkert. Det finns dock astronomer som lever än i dag som kanske inte alltid hade svarat nej på den frågan, dåman för bara ett par årtionden sedan trodde att planeterna formades och utvecklades i sina nuvarance omloppsbanor. Dem första indikationerna på att detta kanske inte var fallet kom inte förrän det sena 1970-talet och tidiga 1980-talet dåbevis för planetmigration upptäcktes. Detta fenomen innebär, enkelt uttryckt, att planeter rör sig närmare eller längre ifrån sin stjärna under sin formation relativt mot vart planeterna börjar formas. Intresset för det tog dock inte fart förrän mitten av 1990-talet med upptäckten av dem första extrasolära planetsystemen eller exosystemen; det vill säga planetsystem i omloppsbana runt en annan stjärna än solen, och i en del av dessa system upptäckten av planeter med så pass underliga omloppsbanor att det var osannolikt att dem hade formats i sina nuvarande positioner. Genom att undersöka den här nu generellt accepterande planetmigrationen kan insikter nås om hur inte bara vårt eget solsystem men även exosystem formades.

Migrationen av väldigt massiva planeter är av särskilt intresse, därav kommer jag i denna avhandling specifikt att titta på hur Jupiter kan ha migrerat under sin formation. Det finns två huvudanledningar till att migrationen av massiva planeter är av särskilt intresse, den första av vilka är att massiva planeter är dem första att formas. För att förstå den andra anledningen behöver vi veta att en ung stjärna är omringad av en disk som består av gas, damm och is som r̈ överblivet från dess formation, och att det är ifrån denna disk som en stjärnas planeter formas. Detta händer då det fasta materialet i disken kan klumpa ihop sig genom turbulenta rörelser och på detta sätt forma de planetära frön som kallas planetesimaler. Dessa planetesimaler är massiva nog att börja dra till sig material från disken genom deras gravitation. Således växer dem än mer massiva vilket i sin tur ökar kraften av deras gravitation. Detta sätter igång en kedjereaktion som för dem mest massiva planeterna lämnar en gas- och dammlös lucka i det område av disken där planeten växer. En sådan lucka påverkar självklart formationen av planeter som växer fram samtidigt eller efter dess formation. Genom att undersöka migrationen av väldigt massiva planeter kan vi således inte bara fåen bättre förståelse för hur den massiva planeten själv formades utan även för hur efterkommande planeter formades. Detta kan i sin tur hjälpa oss att svara på den öppnande frågan och därmed lägga till en bit på pusslet som är den uråldriga frågan om hur vi kom att hamna där vi är.

Contents

List of Figures

List of Tables

List of Symbols

a_0	monomer size [m]
c_s	gas sound speed [m/s]
c_s0	gas sound speed 1 AU from host star [m/s]
D	dust diffusion coefficient [m^2/s]
F_roll	force needed to roll one monomer over the surface of another [kg m/s^2]
G	gravitational constant [m^3/(kg s^2)]
H	disk scale height [m]
H/r	disk aspect ratio [-]
H_p	scale height of pebble layer [m]
k_mig	migration rate prefactor [-]
M	mass of a growing planet [kg]
M_iso	pebble isolation mass [kg]
M_t	transition mass from Bondi to Hill regime [kg]
$M_\star$	mass of the host star [kg]
m	reduced mass of colliding monomers [kg]
$\dot{M}_\mathrm{2D}$	pebble accretion rate in the 2D Hill regime [kg/s]
$\dot{M}_\mathrm{3D}$	pebble accretion rate in the 3D Hill regime [kg/s]
$\dot{M}_\mathrm{disk}$	rate at which gas enters the Hill sphere [kg/s]
$\dot{M}_\mathrm{g}$	gas accretion rate [kg/s]
$\dot{M}_\mathrm{KH}$	Kelvin-Helmholtz gas contraction rate [kg/s]
$\dot{M}_\mathrm{p}$	pebble accretion rate [kg/s]
$\dot{M}_\mathrm{pg}$	gas accretion rate of a gas accreting planet [kg/s]
R	radius of a growing planet [m]
R_acc	accretion radius [m]
R_B	Bondi radius [m]
R_g	characteristic interaction radius [m]
R_H	Hill radius radius [m]
r	radial distance from host star [m]
$\dot{r}$	modified Type-1 migration rate [m/s]
$\dot{r}_1$	Type-1 migration rate [m/s]
St	Stokes number [-]

t_{B}	characteristic timescale to pass a planetesimal in the Bondi regime [s]
t_{H}	characteristic timescale to pass a planetesimal in the Hill regime [s]
t_{s}	characteristic timescale of accretion [s]
$\boldsymbol{u}$	gas velocity [m/s]
u_{f}	critical fragmentation speed [m/s]
u_{r}	gas accretion speed [m/s]
$\boldsymbol{v}$	pebble velocity [m/s]
$\dot{\boldsymbol{v}}$	pebble acceleration due to gas drag [m/s^2]
v_{c}	turbulent collision speed [m/s]
v_{g}	sub-Keplerian speed [m/s]
v_{k}	Keplerian speed [m/s]
Δv_{k}	difference between Keplerian and sub-Keplerian speed [m/s]
v_{r}	pebble radial drift [m/s]
v_{s}	sticking speed [m/s]
α	dimensionless measure of u_{r} and ν [-]
β	negative logarithmic derivative of Σ_{g} [-]
γ	power-law index of turbulent viscosity [-]
δ	dimensionless measure of D [-]
ζ	negative power-law index of the temperature [-]
η	radial pressure parameter [-]
κ	opacity of gaseous envelope [m^2/kg]
ν	turbulent viscosity [m^2/s]
ξ	ratio of pebble and gas accretion rates [-]
$\rho_\bullet$	material density of pebbles [kg/m^3]
ρ_{g}	gas density [kg/m^3]
ρ_{p}	midplane pebble density [kg/m^3]
ρ_{R}	roche density [kg/m^3]
Σ_{g}	gas surface density [kg/m^2]
Σ_{gap}	gas surface density in annular gap [kg/m^2]
Σ_{p}	pebble surface density [kg/m^2]
τ_{f}	friction time [s]
χ	negative logarithmic pressure gradient [-]
Ω	Keplerian frequency [1/s]

Chapter 1

Introduction

In this thesis I simulated the formation and migration of planets as they grew by pebble accretion and subsequent gas accretion up until the dissipation of the protoplanetary disk. These simulations were done using a code developed specifically for the purposes of the thesis. With the help of said simulations I determined the initial parameters of Jupiter analogues in terms of their initial radial distance from their host star and the starting time of their accretion in relation to the lifetime of the disk. This was done to investigate the extent to which Jupiter underwent migration during its formation.

Sections 1.1 and 1.2 below give brief introductions to planetary formation and migration. In chapter 2 we go into detail about the physics behind these phenomena as well as the physics of the disk necessary for the simulations. Chapter 3 gives a short description of how the code functions as well as what was produced by it for the thesis. Also present in chapter 3 is an overview of what parameters were used for the simulations. The results produced by the code are presented in chapter 4 and finally the results and their implications are discussed in chapter 5.

1.1 Planetary formation

Most young stars are surrounded by a disk of gas, dust known as a protoplanetary disk. These disks evolve on million year time scales with the material being accreted by the star. It is generally accepted that it is from these disks that a stars planets form. This stems from the simple facts that not only does their shape reflect the coplanar distribution of material in our solar system but they also contain all the materials necessary for the formation of planets with the average disk having a mass of $0.01 - 0.1\ M_{\odot}$ (Chambers 2009).

The formation of planets is thought to follow multiple steps, beginning with the solid material present in the disk forming larger aggregates, called pebbles, by colliding and

sticking together through turbulent motions. This process of pebble formation is known as coagulation and depending on their density the pebbles formed this way can grow to mm-m sizes. Growth through coagulation is, however, eventually stopped as the pebbles encounter bouncing, fragmentation and radial drift barriers which hinder further growth.

To form planetesimals the pebbles gather in clumps due to the drag they feel from the gas (Johansen et al. 2014). These clumps eventually grow dense enough to collapse under self-gravity. From this point on it has long been thought that further growth towards terrestrial planets and the cores of giant planets is due to the accretion of planetesimals. However, for planetesimal accretion to form planets massive enough to attract a gaseous envelope in the lifetime of the disk surface densities exceeding the minimum mass solar nebula (MMSN) by factor of ten are required (Lambrechts, M. et al. 2014). If that was the case an issue arises as to what happened to the remaining planetesimals not used to create planets.

We will instead consider the relatively new concept of pebble accretion in which mm-cm sized pebbles are the main building blocks for growth beyond the planetesimal size (Ormel & Klahr 2010; Lambrechts & Johansen 2014). Pebbles of these sizes are abundant in the planetary disk due the growth barriers they encounter during coagulation which hinder their growth. The accretion of these pebbles onto the planetesimal takes place in three increasingly efficient regimes which depend on the mass of the planetesimal and the speed of the pebble (see Johansen & Lambrechts 2017, for a review). In the lowest mass regime, known as the geometric regime, pebble accretion is not sufficiently efficient for the planetesimal to grow massive enough to enter the next regime within the lifetime of the disk. As such, planetesimal accretion is assumed to work in tandem with pebble accretion for planetesimals of such low masses. The abundance of pebbles together with the efficiency of pebble accretion in the later stages of Bondi regime as well as in the Hill regime results in planetary growth rates which are several orders of magnitude greater than for planetesimal accretion alone.

As the planetesimal grows into a protoplanet it begins to attract a gaseous envelope due to its increasing mass. However, the heat produced by the flow of pebbles onto the protoplanet keeps the envelope from contracting around it. The continued attraction of gas perturbs the gas density in an annular region around the core, thereby creating a gap in the disk with lower gas density. Protoplanets that grow fast enough become so massive that they reach the so-called pebble isolation mass (Lambrechts, M. et al. 2014). At this mass they gravitationally perturb the gas around them enough to create pressure bumps at the edges of the gap which results in the pebble accretion being halted. With the flow of pebbles stopped the protoplanet cools, thereby lowering the pressure of the gas. This allows the gas to contract and as the pressure due to the heat is no longer a factor the protoplanet can continue gas accretion until the protoplanetary disk dissipates.

The concepts introduced here are expanded upon in chapter 2. However, for a more detailed accounting of planetary formation, including formation by pebble accretion, see Johansen et al. (2014), Lambrechts, M. et al. (2014) and Johansen & Lambrechts (2017).

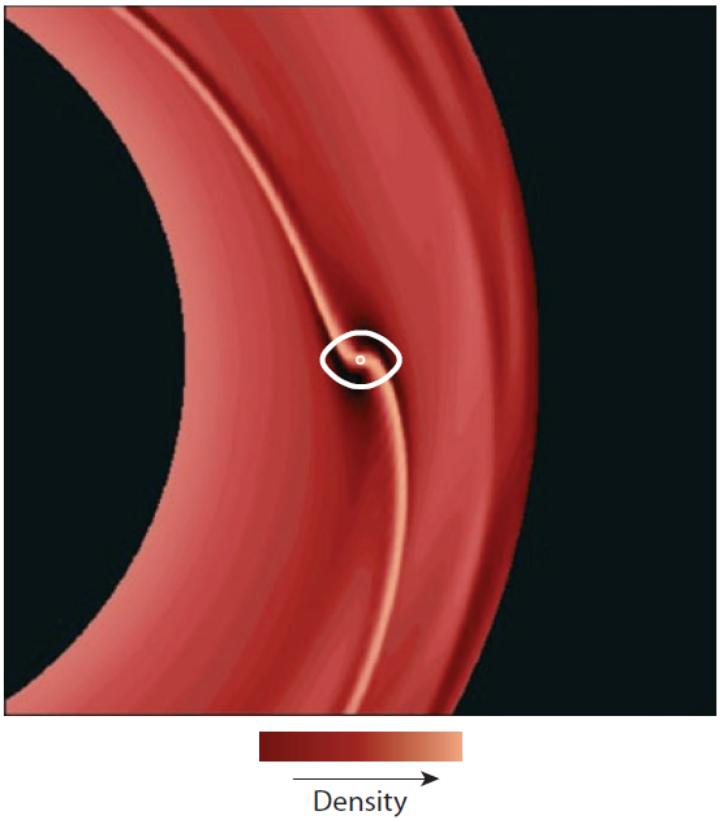

Figure 1.1: Figure 3 from Chambers (2009). Simulation showing the spiral density wakes being excited in the protoplanetary disk by an embedded protoplanet. The protoplanet, located at the center of the plot, is of low mass and is yet to clear an annular gap. Brighter shades indicate higher densities while the inner and outer black regions were not included in the simulation.

1.2 Planetary migration

The orbit of a protoplanet in a protoplanetary disk is subject to change through planetary migration. Like pebble accretion, planetary migration is, in a way, a relatively new concept in planetary science. Although it was first introduced decades ago the subject received little attention until the discovery of exo-planets (Mayor & Queloz 1995; Lin et al. 1996). This newly sparked interest arose as many exo-planets where found with such peculiar orbits that they were unlikely to have formed in situ (Chambers 2009) and planetary migration is now a standard part of planetary formation theories.

This migration stems from gravitational interactions between the protoplanet and the gas in its vicinity. As a result of these interactions spiral density wakes are excited in the gas surrounding the protoplanet. A visualization of such density wakes recreated by a

simulation can be seen in figure 1.1. The inner wake will exert a positive torque on the protoplanet while the outer wake will exert a negative torque. An imbalance between these torques is what drives migration, either towards or away from the host star depending on which way the balance shifts. Migration is generally directed towards the host star, however, the direction is determined by the local properties of the disk and can under certain circumstances be directed away from the star or even halt completely.

Planetary migration is thought to take place in two regimes simply known as Type-1 and Type-2 migration. Low mass protoplanets are subject to Type-1 migration while protoplanets which have accreted enough gas to clear an annular gap in the protoplanetary disk are subject to Type-2 migration. The migration rate in the Type-1 regime is proportional to the mass of the protoplanet in a linear fashion as laid out in section 2.6. At masses above the Earth mass the speed of Type-1 migration is so fast that unless the protoplanet growth rate is sufficiently high the growing planet can migrate to inside 0.1 AU before ever reaching the slower Type-2 regime. This presents a major hurdle for planetary growth through pure planetesimal accretion which can be cleared with the high accretion rates of pebble accretion. This thesis, however, will use a novel solution to the migration rate as laid out by Johansen et al. (2018) in which the protoplanets migrate following a modified version of the classical Type-1 migration.

As will be shown in the thesis it is ultimately the interplay between migration and growth that determines what type of planet, if any, is formed from a growing protoplanet.

Chapter 2

Theory

2.1 Accretion in a protoplanetary disk

Both the gas and the pebbles in the protoplanetary disk accrete onto their host star, however, they do so by different means as detailed in sections 2.1.1 and 2.1.2 below. The accretion rates or mass fluxes of the gas $\dot{M}_{\rm g}$ and the pebbles $\dot{M}_{\rm p}$ are defined in Johansen et al. (2018) as

$$\dot{M}_{\rm g} = -2\pi r u_{\rm r} \Sigma_{\rm g}, \tag{2.1}$$

$$\dot{M}_{\rm p} = -2\pi r v_{\rm r} \Sigma_{\rm p}. \tag{2.2}$$

Here r is the radial distance from the star, u_r is the radial speed of the gas, v_r is the radial speed of the pebbles and Σ_g and Σ_p are the gas and pebble surface densities respectively. Another property I will define here is the ratio of $\dot{M}_g$ and $\dot{M}_p$ denoted as

$$\xi = \frac{\dot{M}_{\rm p}}{\dot{M}_{\rm g}}. \tag{2.3}$$

The accretion rate of the gas is known from Hartmann et al. (1998) to evolve over the disks lifetime as

$$\dot{M}_{\rm g}(t) = \dot{M}_0 \left(\frac{t}{t_{\rm s}} + 1 \right)^{(5/2-\gamma)/(2-\gamma)}. \tag{2.4}$$

In this expression $t_{\rm s}$ is the characteristic timescale of the accretion and through it $\dot{M}_{\rm g}(t)$ is dependent on the turbulent viscosity of the gas ν, a property which will be defined in section 2.1.1. The exponential γ is the power-law index of $\nu \propto r^{\gamma}$ and also enters the expression for $t_{\rm s}$ which is defined as

$$t_{\rm s} = \frac{1}{3(2-\gamma)^2} \frac{R_1^2}{\nu_1} \tag{2.5}$$

where R_1 is the initial radial size of the disk and ν_1 is the value of ν at that radial distance from the star.

2.1.1 Radial drift

Due to a temperature gradient being present in the protoplanetary disk the gas therein is pressure supported in the radial direction. This causes the gas to orbit at a sub-Keplerian speed

$$v_{\mathrm{g}} = v_{\mathrm{k}} - \eta v_{\mathrm{k}} = v_{\mathrm{k}} - \Delta v_{\mathrm{k}} \tag{2.6}$$

where v_{k} is the Keplerian speed and the radial pressure parameter η is given in terms of the radial pressure gradient through

$$\eta \equiv -(1/2)(H/r)^2(\partial \ln P/\partial \ln r). \tag{2.7}$$

Here H is the scale height of the disk and H/r is the disk aspect ratio at the radial distance r from the star.

The scale height H can be expressed as $H = c_{\mathrm{s}}/\Omega$ where c_{s} is the gas sound speed and Ω is the Keplerian frequency. From this expression for H along with 2.6 and 2.7 the reduction in the Keplerian speed of the gas Δv_{k} can be defined as

$$\Delta v_{\mathrm{k}} = -\frac{1}{2}\frac{H}{r}\frac{\partial \ln P}{\partial \ln r} c_{\mathrm{s}}. \tag{2.8}$$

The sound speed in the disk is assumed to follow the power-law expression

$$c_{\mathrm{s}} = c_{\mathrm{s0}} \left(\frac{r}{\mathrm{AU}} \right)^{-\zeta/2} \tag{2.9}$$

where $\zeta = 3/7$ is the negative power-law index of the temperature and $c_{\mathrm{s0}} = 650$ m/s is the sound speed of the gas at 1 AU (Bitsch et al. 2015). Here we also denote the pressure gradient as

$$-\frac{\partial \ln P}{\partial \ln r} \equiv \chi = \beta + \zeta/2 + 3/2 \tag{2.10}$$

where $\beta = 15/14$ is the negative logarithmic derivative of Σ_{g}. This disk profile represents a so-called stellar irradiation disk wherein the heat being supplied to the disk comes solely from the host stars.

The direct effects of the radial pressure on the speed of the pebbles in the protoplanetary disk are negligible. However, the pebbles couple to the gas via drag force with the acceleration of the pebbles due this drag being expressed as

$$\dot{\boldsymbol{v}} = -\frac{1}{\tau_{\mathrm{f}}}(\boldsymbol{v} - \boldsymbol{u}). \tag{2.11}$$

Here $\boldsymbol{v}$ and $\boldsymbol{u}$ are the pebble and gas velocities respectively and $\tau_{\rm f}$ is the friction time of the pebbles with the gas (Johansen et al. 2014). As the gas travels at a sub-Keplerian speed, the drag on the pebbles (which initially orbits with the Keplerian speed $v_{\rm k}$) serves to decelerate them. Accretion of the pebbles onto the host star is then due to this deceleration as it continually lowers their angular momentum.

The friction time τ_f can be divided into different regimes that depend on the mean free path of the gas as well as the speed of the pebbles in relation to the gas ($\boldsymbol{v} - \boldsymbol{u}$). For a detailed description of the different friction regimes see Johansen et al. (2014). I will focus on pebbles in the Epstein regime which is valid when the size of the pebbles is smaller than the mean free path of the gas. In this regime the expression for $\tau_{\rm f}$ is independent of the relative speed and is given by

$$\tau_{\rm f} = \frac{R\rho_\bullet}{c_{\rm s}\rho_{\rm g}}. \tag{2.12}$$

Here R is the radius of the pebble which is assumed to spherical while $\rho_\bullet$ and $\rho_{\rm g}$ is the material density of the pebble and the gas density respectively. The radial drift speed of the pebbles $v_{\rm r}$ is dependent on $\tau_{\rm f}$ through the Stokes number ${\rm St} = \tau_{\rm f}\Omega$ and is given by

$$v_{\rm r} = -\frac{2\Delta v_{\rm k}}{{\rm St} + {\rm St}^{-1}} + \frac{u_{\rm r}}{1 + {\rm St}^2}. \tag{2.13}$$

In the limit that ${\rm St} \ll 1$, which is valid for all simulations performed in this thesis, 2.13 simplifies to

$$v_{\rm r} = -2{\rm St}\Delta v_{\rm k} + u_{\rm r}. \tag{2.14}$$

The dimensionless Stokes number introduced for 2.13 is a useful parameter to define as $1/\Omega$ is the natural timescale for physical effects in a protoplanetary disk and $\tau_{\rm f}$ contains all the physics of the pebble and gas interaction. As such St not only enters into the expression for $v_{\rm r}$ but plays a part in all interactions between the gas and the pebbles.

2.1.2 Gas accretion

Accretion of gas onto the host star is due to the diffusion of the angular momentum of the gas in the faster moving inner parts of the protoplanetary disk to the gas in the slower moving outer parts. The radial speed of the gas due to this diffusion is proportional to the turbulent viscosity ν in the disk which is itself determined by both $c_{\rm s}$ and H. In this thesis I use the $\alpha-$disk assumption which gives the following expression for the turbulent viscosity

$$\nu = \alpha c_{\rm s} H = \frac{\alpha c_{\rm s}^2}{\Omega}. \tag{2.15}$$

This in turn results in the gas accretion speed

$$u_{\rm r} = -\frac{3}{2}\frac{\nu}{r} = -\frac{3}{2}\alpha c_{\rm s}\frac{H}{r} \tag{2.16}$$

where α is simply a dimensionless measure of u_r. If the angular momentum loss of the gas was instead caused by disc winds (Bai & Stone 2013) this expression for u_r would not be valid as it is specific to the α-model assumption.

2.2 Pebble growth

Pebble growth is a consequence dust particles coagulating into larger aggregates due to turbulent motions. For dust particles and pebbles with $\mathrm{St} < 1$ the turbulent collision speed v_c is set by the Stokes number through

$$v_\mathrm{c} = c_\mathrm{s}\sqrt{3\alpha_\mathrm{v}\mathrm{St}}. \tag{2.17}$$

Here α_v is a dimensionless measure of the turbulent viscosity which is to be distinguished from α as α may be driven by disc winds at a weak level of actual turbulence (Bai & Stone 2013). Depending on the internal structure and composition of the particles the growth from these collisions is eventually halted as the growing aggregates encounter one of the three coagulation barriers.

2.2.1 Fragmentation barrier

The fragmentation barrier is reached when v_c becomes equal to the critical fragmentation speed u_f at which point colliding particles fragment rather than stick together (Birnstiel et al. 2011). This gives an expression for the Stokes number at which the barrier is encountered through 2.17 as

$$\mathrm{St} = \frac{u_\mathrm{f}^2}{3\alpha_\mathrm{v}c_\mathrm{s}^2}. \tag{2.18}$$

As mentioned in Johansen & Lambrechts (2017) u_f is a complicated function of the porosity and size of the colliding particles. However, it can for simplicity to be set to a constant to obtain an approximate solution to the Stokes number of the fragmentation barrier.

2.2.2 Bouncing barrier

The speed at which particles can stick together through coagulation is limited by what is known as the sticking speed v_s defined as

$$v_\mathrm{s} = \sqrt{\frac{5\pi a_0 F_\mathrm{roll}}{m}}. \tag{2.19}$$

Here a_0 is the size of the pebble building blocks, known as a monomer, F_roll is the force needed to roll one monomer over the surface of another and m is the reduced mass of the

colliding monomers. Particles that collide with collision speeds equal to this sticking speed bounce of each other rather than stick together (Zsom et al. 2010). As this expression is inversely proportional to m the growth of high density particles made from silicates will be hindered by bouncing before they begin to fragment.

2.2.3 Radial drift barrier

If a particle can grow large enough without reaching the fragmentation or sticking speed it will eventually cease growth due to its radial drift. This happens for low density pebbles such as very fluffy ice aggregates when their radial drift timescale $r/\dot{r}$ equals their growth timescale $\mathrm{St}/\dot{\mathrm{St}}$ (Birnstiel et al. 2011; Lambrechts & Johansen 2014). The fate of these icy aggregates is not to fall into the star however, but rather to evaporate and sublimate at different snow lines whose radial position in the disk depends on the composition of the ice. Pebble formation can take place at these snow lines through the condensation of the ice vapor onto already existing ice particles (Ros & Johansen 2013; Johansen et al. 2014). This type of pebble formation is not pertinent to this thesis however so I will not go into further detail about it.

2.3 Planetesimal formation

As the pebbles grow they begin to sediment towards the midplane of the protoplanetary disk. Due to sedimentation being counteracted by turbulent diffusion the pebbles eventually settle in an equilibrium midplane layer as the two reach a balance. The scale height of this midplane pebble layer H_p can be expressed in terms of the gas scale height H through

$$H_\mathrm{p} = H\sqrt{\frac{\delta}{\mathrm{St}+\delta}} \tag{2.20}$$

where δ is a dimensionless measure of the dust diffusion coefficient $D = \delta c_\mathrm{s} H$. If the pebble density exceeds the Roche density

$$\rho_\mathrm{R} = \frac{9\Omega^2}{4\pi G}, \tag{2.21}$$

where G is the gravitational constant, the pebbles can contract to form a planetesimal held together by self-gravity. However, sedimentation alone will not lead to pebble densities that fulfill this criteria due to the turbulent diffusion. Instead, the pebbles can concentrate locally due to turbulent motions and so-called streaming instabilities. In both of these cases the concentration of pebbles is due to their radial drift being locally slowed down or even halted completely.

Turbulent motions can lead to regions in the protoplanetary disk where the gas speed goes from sub- to super-Keplerian. The positive drag felt by the pebbles as they enter the super-Keplerian gas accelerates them back towards the sub-Keplerian gas. This creates a pebble trap where $\Delta v_{\mathrm{k}} = 0$ in which the local pebble density can grow towards ρ_{R}. Streaming instabilities on the other hand are due to instabilities in the local radial drift speed of the pebbles. These instabilities can lead to perturbations in the local pebble density. If the local pebble density is increased by such a perturbation the gas in the region will feel an increased positive drag force from the pebbles. As the local gas speed grows closer to v_{k} due to this increased drag the local radial drift speed decreases. This can lead to streaming instabilities, as seen in figure 2.1, wherein the pebbles begin to pile up due to the decrease in the local radial drift speed. As more and more pebbles arrive the local gas and radial drift speeds keep increasing and decreasing respectively leading to local pebble densities which exceed ρ_{R}. In this way large planetesimals with contracted radii between 100-1000km are formed (Johansen et al. 2014).

2.4 Pebble accretion

Planetesimals have long been thought to continue their growth towards terrestrial planets and planetary cores through the accretion of other planetesimals. However, due to the gas drag and resulting angular momentum loss experienced by pebbles as they pass by the growing planetesimals and protoplanets they are more readily accreted than planetesimals. Pebbles are also abundant in the protoplanetary disk as the coagulation barriers makes the disk efficient at producing them. This accretion efficiency and abundance of pebbles makes pebble accretion an interesting alternative to planetesimal accretion.

Pebble accretion, which is the focus of this thesis, can take place in either the geometric, the Bondi or the Hill regime. These regimes are determined by the characteristic interaction radius R_{g} of the planetesimal which is given by

$$R_{\mathrm{g}} = \frac{GM}{\delta v^2}. \tag{2.22}$$

where M is the mass of the growing planetesimal and δv is the relative speed of passing pebbles. The Bondi radius R_{B} is given by this expression when δv is dominated by Δv_{k} while the Hill radius R_{H} is obtained when δv is dominated by the Hill speed $v_{\mathrm{H}} = \Omega R_{\mathrm{H}}$. A transition mass M_{t} from the Bondi regime to the Hill regime can then be extracted from 2.22 by equating Δv_{k} with $v_{\mathrm{H}} = \Omega R_{\mathrm{H}}$

$$M_{\mathrm{t}} = \sqrt{\frac{1}{3}} \frac{\Delta v_{\mathrm{k}}^3}{G\Omega}. \tag{2.23}$$

This gives a transition mass typically ranging between $1.5 \times 10^{-4} - 1.2 \times 10^{-2}$ $\mathrm{M_E}$ where M_{E} is the Earth mass.

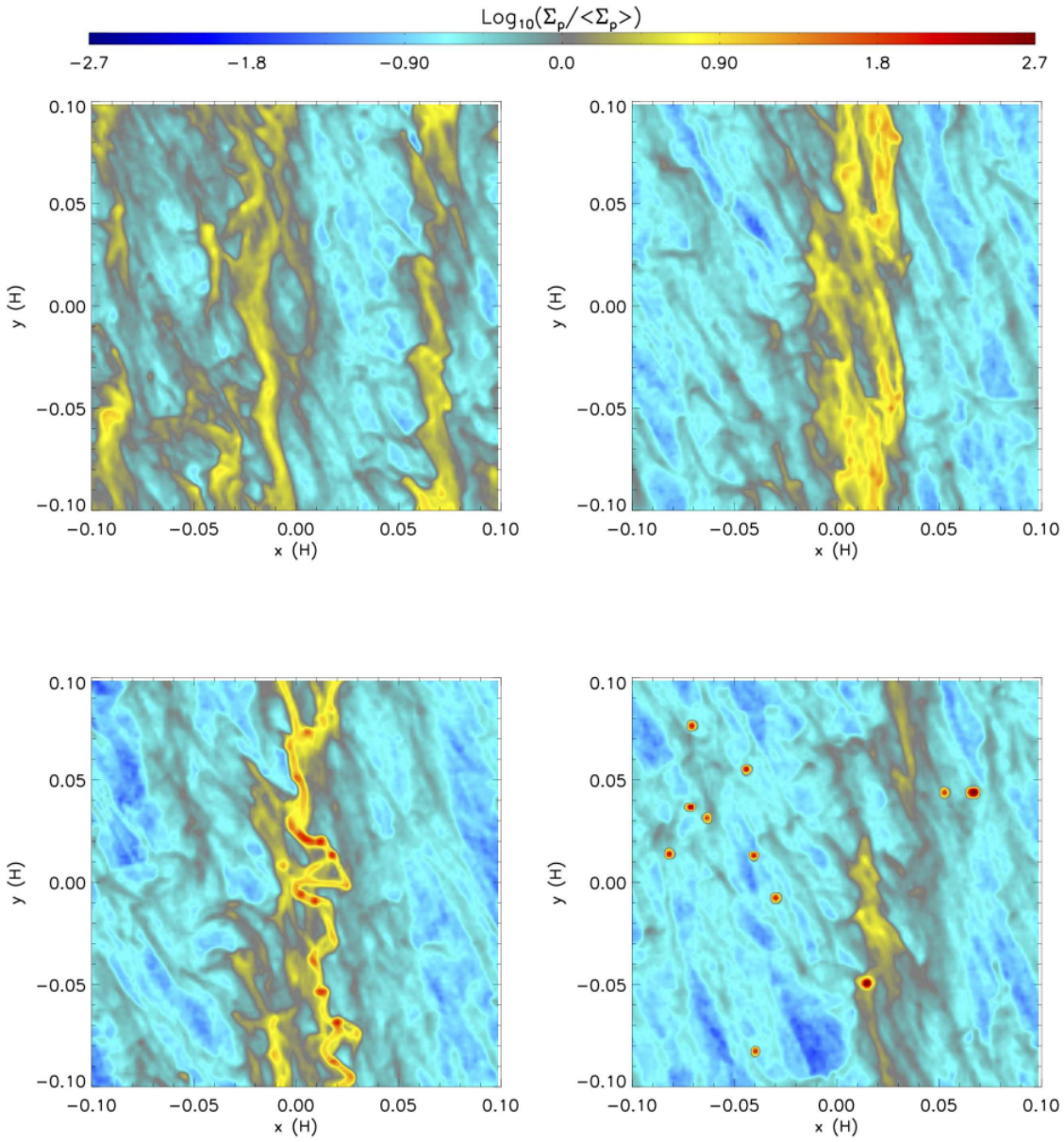

Figure 2.1: Figure 7 from (Simon et al. 2016). Formation of a streaming instability and the subsequent formation of planetesimals. The density has been normalized by the average pebble surface density in the protoplanetary disk and the axes have been normalized by H. Four sequential snapshots in time are shown from the top left to the bottom right. In the bottom left plot pebbles beginning to collapse through self-gravity can be seen while in the bottom right planetesimals have formed and the streaming instability has almost completely dissolved.

2.4.1 Bondi regime

The accretion radius of a planetesimal $R_{\rm acc}$ is a function of $R_{\rm g}$ as well as $\tau_{\rm f}$ relative to the characteristic timescale to pass the planetesimal. However, $R_{\rm acc}$ also depends on which regime the planetesimal is accreting in. In the Bondi regime, also known as the drift regime due to the approach speed of pebbles being set by their drift speed, $R_{\rm acc}$ is given by

$$R_{\rm acc} = \left(\frac{4\tau_{\rm f}}{t_{\rm B}}\right)^{1/2} R_{\rm B} \tag{2.24}$$

where $t_{\rm B} = R_{\rm B}/\Delta v_{\rm k}$ is the characteristic timescale to pass a planetesimal in the Bondi regime. Figure 2.2 shows pebbles with $\tau_{\rm f} = 100 t_{\rm B}$, $\tau_{\rm f} = t_{\rm B}$ and $\tau_{\rm f} = 0.1 t_{\rm B}$ approaching a planetesimal in the Bondi regime. Weakly coupled pebbles with $\tau_{\rm f} = 100 t_{\rm B}$ are scattered by the planetesimal owing to the weak drag they feel while optimally coupled pebbles with $\tau_{\rm f} = t_{\rm B}$ enter decaying orbits around the planetesimal and are accreted from within most of $R_{\rm B}$. Pebbles with $\tau_{\rm f} < t_{\rm B}$ can be accreted as well though from smaller impact parameters than optimally coupled pebbles.

2.4.2 Geometric regime

Planetesimals whose physical radius R is greater than $R_{\rm B}$ will accrete in the geometric regime characterized by the timescale to pass the planetesimal $R/\Delta v_{\rm k}$. Here the planetesimal has a capture radius which is equal to its own size and pebbles approach with a speed that is greater than the escape speed of the planetesimal. This can result in weakly coupled pebbles escaping the planetesimal when colliding with it elastically. The momentum loss of the pebbles in inelastic collisions can however lead to accretion of weakly coupled pebbles if their new speed is lower than the escape speed. Optimally coupled pebbles are accreted in both elastic and inelastic collisons as the gas drag is sufficient to lower their speeds below the escape speed. The accretion of strongly coupled pebbles in this regime is more complicated. These pebbles enter a decaying orbit around the planetesimal resulting in an accretion efficiency which depends on both $\tau_{\rm f}$ and the gas flow pattern.

Pebble accretion in the geometric regime and early stages of the Bondi regime is not sufficiently efficient for a planetesimal to grow to planet size within the lifetime of the protoplanetary disk. As such, planetesimal accretion is a necessary complement to pebble accretion at these stages.

2.4.3 Hill regime

When a planetesimal has become massive enough to enter the Hill regime it is known as a protoplanet. At this point the timescale to pass the protoplanet is $t_{\rm H} = \Omega^{-1}$ independent

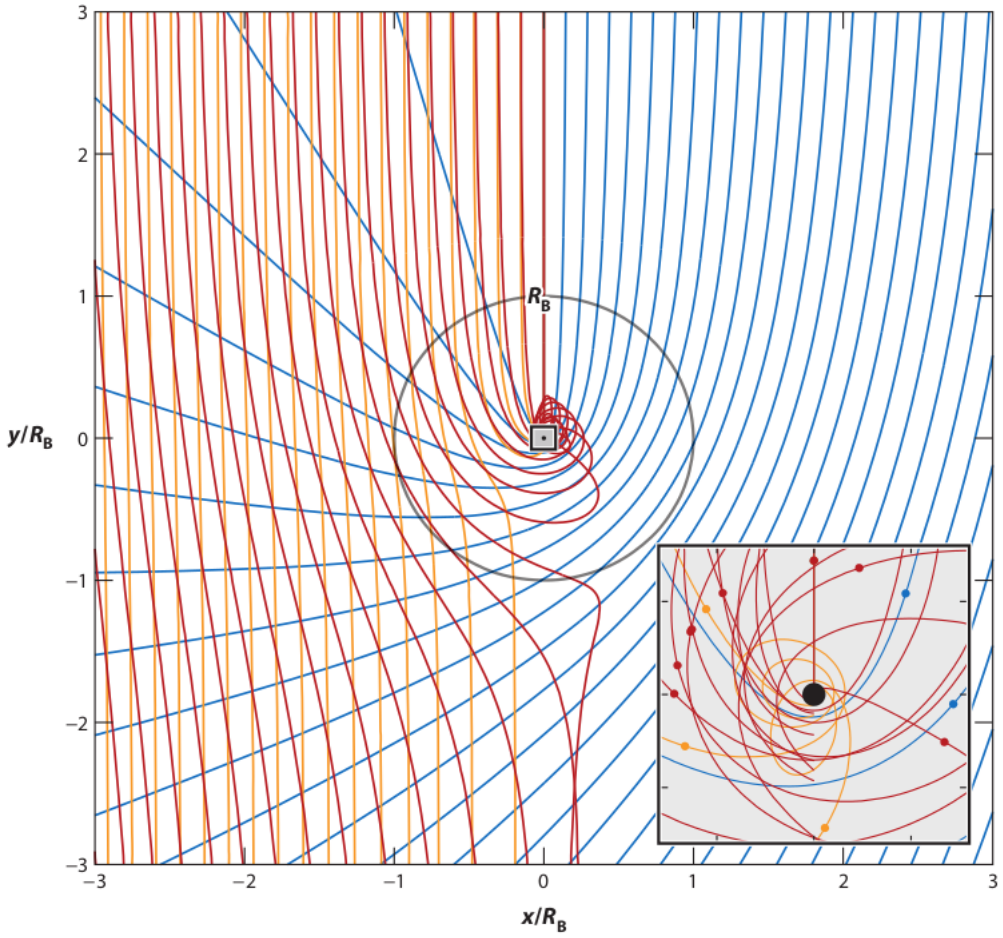

Figure 2.2: Figure 1 from Johansen & Lambrechts (2017). Pebble accretion in the Bondi regime. Blue trajectories show weakly coupled pebbles ($\tau_{\rm f} = 100 t_{\rm B}$), red trajectories show optimally coupled pebbles ($\tau_{\rm f} = t_{\rm B}$) and orange trajectories show strongly coupled pebbles ($\tau_{\rm f} = 0.1 t_{\rm B}$). The scattering of weakly coupled pebbles as well as the decaying orbits of optimally and strongly coupled pebbles can be seen in the inset where colored dots mark incoming trajectories. The axes are normalized by $R_{\rm B}$ and the pebbles enter from above with $\Delta v_{\rm k}$.

of the protoplanet mass and the approach speed of the pebbles is set by the Keplerian shear flow. As a result of $t_{\rm H}$ being equal to the inverse of the Keplerian frequency $R_{\rm acc}$ is determined by St in the Hill regime with the expression for $R_{\rm acc}$ being given by Johansen & Lambrechts (2017) as

$$R_{\rm acc} = \left(\frac{\rm St}{0.1} \right)^{1/3} R_{\rm H}. \tag{2.25}$$

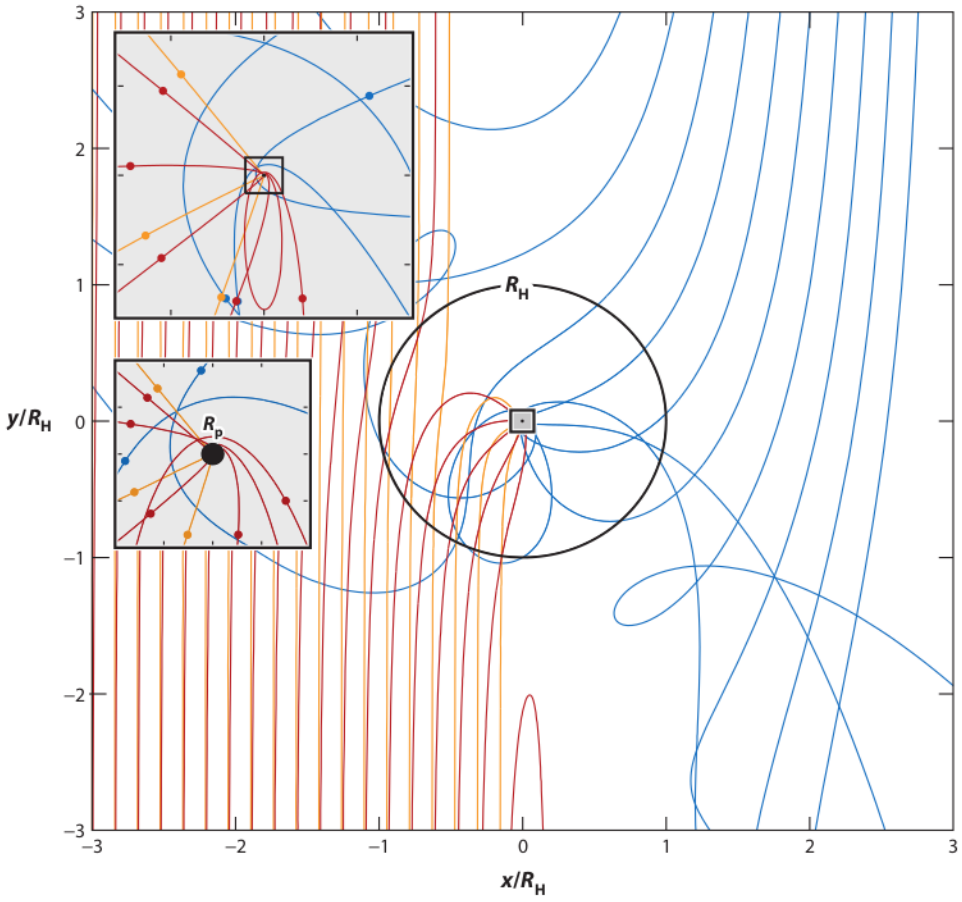

Figure 2.3: Figure 2 from Johansen & Lambrechts (2017). Pebble accretion in the Hill regime. The axes are normalized by R_{H}. Blue trajectories show very large pebbles that couple to the gas on a timescale which is much longer than the orbital timescale. These weakly coupled pebbles are scattered by the protoplanet. Red trajectories show optimally coupled pebbles with $\mathrm{St} = 1$ while orange trajectories show strongly coupled pebbles with $\mathrm{St} = 0.1$. The protoplanet accretes optimally and strongly coupled pebbled from within most of R_{H}. Optimally coupled pebbles entering horseshoe orbits can be seen in the two insets. As the protoplanet radius is just 0.001 times its Hill radius the insets are shown at two different scales.

The trajectories of pebbles in the Hill regime can be seen in figure 2.3. As in the Bondi regime, the weakly coupled pebbles are scattered by the protoplanet while optimally and strongly coupled pebbles are accreted. However, the dynamics of the pebble trajectories are heavily influenced by the Coriolis force in the Hill regime. This can lead to pebbles with low impact parameters entering horseshoe orbits around the protoplanet as can be seen in the figure 2.3 insets.

Pebble accretion in the Hill regime is said to be either 3-dimensional or 2-dimensional depending on the relation between $R_{\rm acc}$ and the scale height of the pebble layer $H_{\rm p}$. The accretion is 3-dimensional when $R_{\rm acc}$ is smaller than $H_{\rm p}$. If this criteria is fulfilled the accretion rate $\dot{M}_{\rm 3D}$ can be expressed as

$$\dot{M}_{\rm 3D} = \pi \left(\frac{\rm St}{0.1} \right) \Omega R_{\rm H}^3 \rho_{\rm p} \tag{2.26}$$

where $\rho_{\rm p} = \Sigma_{\rm p}/(\sqrt{2\pi} H_{\rm p})$ is the midplane pebble density. Should $R_{\rm acc}$ grow larger than $H_{\rm p}$ the accretion becomes 2-dimensional in which case the accretion rate can be expressed as.

$$\dot{M}_{\rm 2D} = 2 \left(\frac{\rm St}{0.1} \right)^{2/3} \Omega R_{\rm H}^2 \Sigma_{\rm p}. \tag{2.27}$$

2.4.4 Isolation Mass

As the planetesimal and eventual protoplanet grows through pebble accretion it begins to attract a gaseous envelope due to its increasing gravitational pull. Heat supplied by the accreted pebbles keeps the continually growing envelope pressure supported and thus it can not contract around the core. The continued attraction of gas perturbs the gas density in an annular region around the core, thereby creating a gap with lower gas density as seen in figure 2.4.

When the protoplanet mass reaches the pebble isolation mass $\dot{M}_{\rm iso}$ the perturbations become so great that pressure bumps are formed at the edges of the annular region. As in the formation of planetesimals the reversing of the pressure gradient creates a pebble trap which abruptly halts the pebble accretion onto the protoplanet (possibly resulting in a new planetesimal formation zone). Bitsch et al. (2018) determined that $\dot{M}_{\rm iso}$ follows

$$M_{\rm iso} = \left(\frac{H/r}{0.05} \right)^3 \left(0.34 \left(\frac{\log(\alpha_3)}{\log(\alpha_{\rm v})} \right)^4 + 0.66 \right) \left(1 - \frac{2.5 + \chi}{6} \right) \tag{2.28}$$

where $\alpha_3 = 0.001$ is a constant.

2.5 Protoplanet gas accretion

As the protoplanet cools due to the lack of heat being supplied by pebble accretion the gaseous envelope surrounding it can contract. The contraction of the envelope subsequently heats the protoplanet again. This Kelvin-Helmholtz like contraction of the envelope results

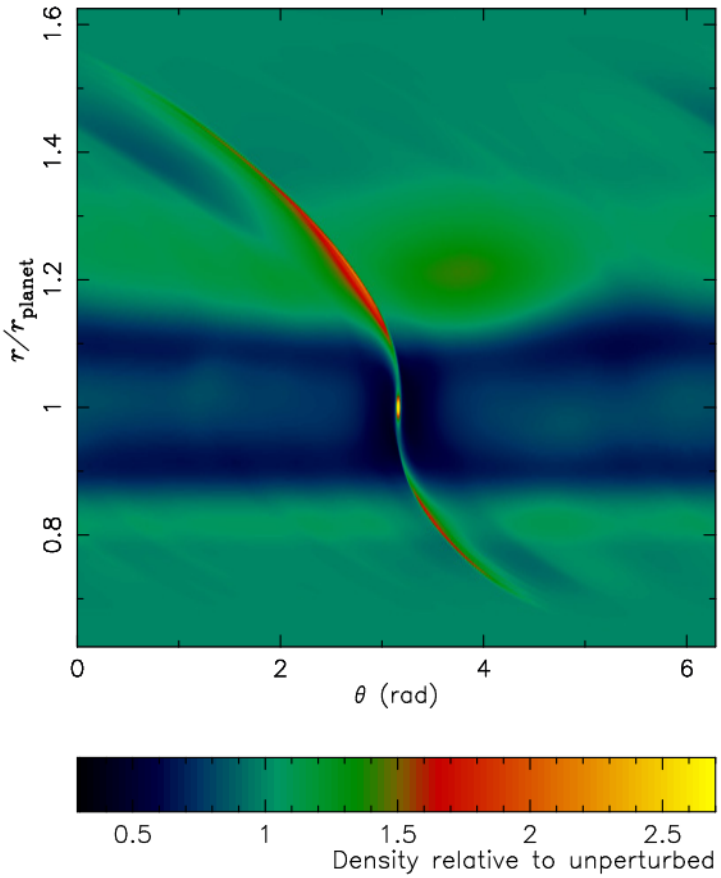

Figure 2.4: Figure 2 from (Lambrechts, M. et al. 2014). Annular gap cleared by a planet with $M = 50M_{\rm E}$ embedded in the midplane of a protoplanetary disk. The x-axis is normalized by the radial distance of the planet from the host star. $M_{\rm iso}$ has been reached and pebble accretion has been completely halted. The densities exceeding the unperturbed density seen interior and exterior to the gap are regions where the gas orbits with a super-Keplerian speed due to the perturbations caused by the presence of the massive planet.

in the gas accretion rate (Ikoma et al. 2000)

$$\dot{M}_{\rm KH} = \frac{10^{-5}\, M_{\rm E}}{\rm yr} \left(\frac{M}{10\, M_{\rm E}} \right)^4 \left(\frac{\kappa}{0.1\ {\rm m^2\ kg^{-1}}} \right)^{-1} \tag{2.29}$$

where κ is the opacity of the envelope. However, as $\dot{M}_{\rm KH} \propto M^4$ this rate increases rapidly and is eventually limited by the rate at which gas enters the Hill sphere

$$\dot{M}_{\rm disk} = \frac{0.29}{3\pi} \left(\frac{H}{r} \right)^{-4} \left(\frac{M}{M_\star} \right)^{4/3} \frac{\dot{M}_{\rm g}}{\alpha} \frac{\Sigma_{\rm gap}}{\Sigma_{\rm g}} \tag{2.30}$$

where $\Sigma_{\rm gap}$ is the gas surface density in the gap and $M_\star$ is the mass of the host star. The gas accretion onto the protoplanet becomes further limited if $M_{\rm disc}$ grows large enough within the lifetime of the disk to completely absorb $\dot{M}_{\rm g}$. This results in a protoplanet gas accretion rate $\dot{M}_{\rm pg}$ that is ultimately set by

$$\dot{M}_{\rm pg} = \min\left(\dot{M}_{\rm KH}, \dot{M}_{\rm disc}, \dot{M}_{\rm g}\right). \tag{2.31}$$

2.6 Planetary migration

Perturbations to the gas flow caused by the gravity of a growing planet leads to spiral density wakes being launched in the gas around it as demonstrated in figure 1.1. The wake on the planets exterior in relation to the host star will carry angular momentum away from the planet by exerting a negative torque on it. For the wake on the planets interior the situation is reversed. The mechanics behind the launching of these wakes and the angular momentum being carried by them are quite complex and beyond the scope of this thesis. I instead refer to Chambers (2009), Nelson (2018) and Kanagawa et al. (2018) for a more in depth review on the subject. Here it will suffice to say that the momentum being carried away from the growing planet is under ordinary circumstances greater than the momentum being carried to it. As a result a net negative torque is exerted on the planet which leads to inwards migration.

This type of migration is what is called Type-1 migration and the migration rate due to the momentum loss follows

$$\dot{r}_1 = -k_{\rm mig}\frac{M}{M_\star}\frac{\Sigma_{\rm g} r^2}{M_\star}\left(\frac{H}{r}\right)^{-2} v_{\rm K} \tag{2.32}$$

where $M_\star$ is the mass of the host star (Johansen et al. 2018). The prefactor $k_{\rm mig}$ is a constant which depends on the gradients of surface density β and temperature ζ. Simulations performed by D'Angelo & Lubow (2010) found that $k_{\rm mig}$ is given by

$$k_{\rm mig} = 2(1.36 + 0.62\beta + 0.43\zeta). \tag{2.33}$$

Should the gas flow through the annular gap created as the protoplanet grows completely halt the protoplanet will be subject to Type-2 migration. At this point the protoplanet becomes locked inside the gap as migration towards either of the edges leads to an imbalance in the torque acting on it which pushes the protoplanet back to the middle of the gap (Chambers 2009). This means that the migration rate in the Type-2 regime is equal to the gas accretion rate as the protoplanet is essentially pushed along by the gas.

2.6.1 Modified Type-1 migration

Recent simulations have shown that gas can continue to flow through the gap and that subsequently the migration rate is not tied to the gas accretion (Kanagawa et al. 2018). These simulations found instead that the torque on a growing planet can be described by the classical Type-1 torque multiplied by the relative gap depth $\Sigma_{\rm gap}/\Sigma_{\rm g}$. A good fit to an expression for the relative gap depth is given by (Johansen et al. (2018))

$$\frac{\Sigma_{\rm gap}}{\Sigma_{\rm g}} = \frac{1}{1+0.04K} \tag{2.34}$$

where

$$K = \left(\frac{M}{M_\star}\right)^2 \left(\frac{H}{r}\right)^{-5} \alpha_{\rm v}^{-1}. \tag{2.35}$$

This yields a migration rate which can be expressed as (Johansen et al. 2018)

$$\dot{r} = \frac{\dot{r}_1}{1+(M/M_{\rm gap})^2}. \tag{2.36}$$

Here $M_{\rm gap}$ is the gap transition mass, defined as the mass for which $K = 1/0.04$ and as such the mass which is required to create a relative gap depth of 0.5. To reach $M_{\rm iso}$ a relative gap depth of 0.85 is sufficient from which Johansen et al. (2018) finds that $M_{\rm gap} = 2.3 M_{\rm iso}$.

Chapter 3

Method

3.1 Code

To simulate the growth and migration of protoplanets I developed a code in `Python` which numerically integrates their mass and radial position according to the Euler method. All simulations performed for the thesis using this code started with a protoplanet mass of $M = 0.01$ $M_\oplus$ and the simulated protoplanets were assumed to begin accretion in the 2D Hill-regime. Furthermore the protplanets were assumed to migrate according to the migration model laid out by Johansen et al. (2018). As such, the code was developed to utilize Eq. 2.36 for the numerical integration of the radial position and Eq. 2.27 for the numerical integration of the mass. Should the mass of a growing planet reach M_{iso} in the simulations Eq. 2.31 takes precedence over 2.27 in the code as further mass increase to is due to gas contraction. For the interested reader Appendix A presents a link to a github-repository which contains all of the code developed for the thesis.

Using this code I produced growth tracks in which I show how the mass of the growing planet evolves with its radial distance from host star. These growth tracks were initiated with a starting radial distance as well as starting time in relation to the lifetime of the disk. The simulations then continued up until the dissipation of the protoplanetary disk following static values for α, St and ξ. These parameters as well as all other parameters necessary for the simulations are detailed in section 3.2.

Growth maps which show the final positions and masses of the simulated protoplanets as overlapping contours were produced using the same code developed to produce the growth tracks. The coordinates of these growth maps which are represented by the initial distance from the host star r_0 and the starting time t_0 range from 1-60 AU and 0-3 Myrs respectively. With the help of a `Python` module called `shapely` I determined r_0 and t_0 for possible Jupiter analogues from said growth maps. This could be done as `shapely` can be utilized to find the coordinates of an intersection between two contours. By taking

advantage of this functionality present in `shapely` I determined the coordinates of the intersection between the Jupiter mass (318 M_E) contour and the Jupiter position (5.2 AU) contour for different protoplanetary disk parameters.

An altered version of the code in which the numerical integrations were done according to the more accurate Runge-Kutta method, as compared to the Euler method, was also developed. This was done so that the accuracy of the Euler method could be investigated.

An altered version of the code in which the numerical integrations were done according to the more accurate Runge-Kutta method, as compared to the Euler method, was also developed. Using this version of the code I determined the final mass and radial position values of planets evolving according to the same parameters used for the growth tracks produced by the Euler version of the code so that the accuracy of the Euler method could be investigated.

3.2 Simulation parameters

In the protoplanetary disk model used for the simulations of the thesis I followed the standard viscous accretion disk model where $\dot{M}_g$ drops from $10^{-7}M_\odot$/yr to $10^{-8}M_\odot$/yr according to Eq. 2.4 over 3 Myr. As such, Σ_g evolves with $\dot{M}_g$ in contrast to the MMSN where it is assumed to follow $1700(r/\mathrm{AU})^{-3/2}$ g/m^2 (Hayashi 1981). In figure 3.1 plots produced by the code can be found which show the dependence of Σ_g on r due to this accretion rate as compared to the MMSN for two different values of α.

After these 3 Myr the disk is assumed to dissipate with most of the material having been accreted on to the star. From this $\dot{M}_p$ and subsequently Σ_p can obtained through 2.3 where ξ is a static parameter which was set for each simulation.

The gas accretion rate used in the simulations produces pebbles whose sizes are typically in the mm-cm range for $\mathrm{St} = \alpha$. These sizes fall well in line with pebbles which have further growth hindered by the bouncing barrier. Pebbles which are that small have radial speeds that are approximately the same as the gas accretion speed. This results in the solid and gaseous components of the protoplanetary disk being depleted on similar time scales. As such, I used $\mathrm{St} = \alpha$ in all simulations. This choice is justified by the fact that it agrees well with both the bouncing barrier as well as with observations which show mm-cm sized pebbles remaining present in protoplanetary disks over a wide range of ages (Johansen et al. 2018).

Any dependence of a protoplanets inclination and eccentricity on pebble accretion rates is not yet well understood, though significant effort is currently being put into it. Therefore it was not taken into account in any simulations and I instead focused on the simpler case of a protoplanet on a circular orbit.

The gas accreted onto protoplanets which have reached M_{iso} is assumed to be completely

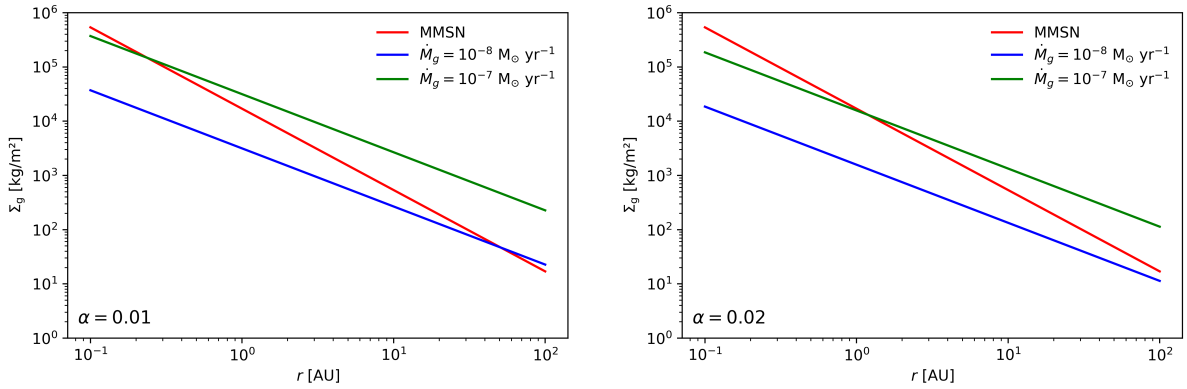

Figure 3.1: Gas surface density as a function of r in a disk following the standard viscous accretion model. Both the left and right plot display the gas surface density at the beginning of the lifetime of the disk (green) as well as after 3 Myr (blue) though they do so for two different values of α. The gas surface density of the MMSN (red) is shown as a comparison in both plots.

pebble free due to the pressure bump created at the edge of the gap. In spite of this small dust particles can still pass the gap along with the accreted gas. These dust particles can constitute 10% of the total content of solids resulting in a nominal opacity in the range 0.001-0.01 m^2 kg^{-1} (Johansen et al. 2018). Therefore a standard opacity value of $\kappa = 0.005$ m^2 kg^{-1} was used for all simulations.

Finally, the time step of $\mathrm{dt}_{\mathrm{gt}}$ of the numerical integration performed by the code using the Euler method was set to follow

$$\mathrm{dt}_{\mathrm{g}} = 0.01 \cdot \min\left(\frac{M}{\dot{M}}, \frac{r}{\dot{r}}\right) \tag{3.1}$$

for the growth tracks. Here $\dot{M}$ is the accretion rate of the type of accretion the protoplanet is subject to at the current point in the simulation. Thus the size of the time-step decreased as either the protoplanets growth or migration rate increased in relation to its mass and radial position respectively. This procedure for determining the time-step was chosen as compromise between the computation time of the simulations and their accuracy. The simulations producing the growth maps on the other hand required a higher accuracy for the contours to come out smooth. Thus the time step for these simulations $_{\mathrm{gm}}$ was set to follow

$$\mathrm{dt}_{\mathrm{gm}} = \min\left(\mathrm{dt}_{\mathrm{g}}, 100 \text{ yr}\right). \tag{3.2}$$

Chapter 4

Results

4.1 Growth tracks

Growth tracks produced by the code for four different pairs of ξ and α/St values starting at $r_0 = 10$ AU and $r_0 = 30$ AU are presented in figure 4.1. The figure presents two different plots, one of which shows growth tracks which were initiated at $t_0 = 0.7$ Myr while the other shows growth tracks which were initiated at $t_0 = 1.2$ Myr. The protoplanets responsible for the growth tracks in both of these plots form in protoplanetary disk with the same values for α, St and ξ. This is done in order to show the effects of the starting time on the growth tracks.

The final masses and radial positions of the planets represented by the growth tracks initiated at $t_0 = 0.7$ Myr and $r_0 = 30$ AU are presented in table 4.1. This table also presents the final masses and radial positions of planets were the numerical integrations were done using the Runge-Kutta method for the same initial parameters.

Looking at the growth tracks one can see that the distance travelled by a protoplanet due to migration before reaching M_{iso} increases rapidly as the starting location moves farther from the host star. This phenomenon arises from r_{iso} being proportional to r_0 through $r_{\mathrm{iso}} \propto r_0^{1/2}$ where r_{iso} is the radial position at which M_{iso} is reached. For a derivation of this proportionality see sections 2.5-7 of Johansen et al. (2018).

Initially the migration seen in the growth tracks essentially follows the classical Type-1 migration as $M \ll M_{\mathrm{gap}}$. As such, the growth tracks grow ever more horizontal as the protoplanets represented by them grow more massive. However, as can be seen all but one of the tracks that manage to reach M_{iso} abruptly turn more vertical at some point after doing so. The protoplanets responsible for these tracks are massive enough for Kelvin-Helmholtz contraction to be effective. This results in the protoplanets quickly growing so massive that the migration rate, which is inversely proportional to M, rapidly drops. For lower mass protoplanets the Kelvin-Helmholtz contraction is significantly less effective due

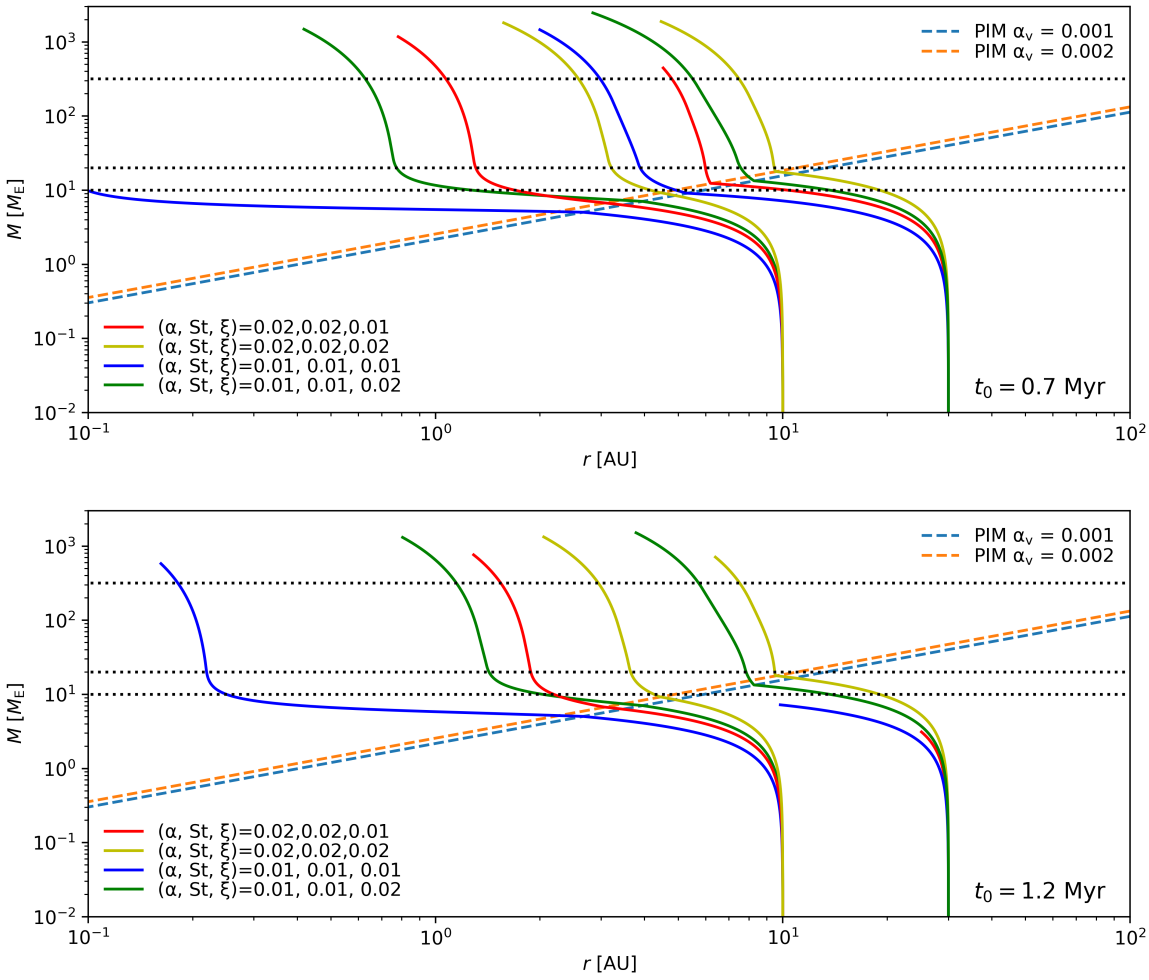

Figure 4.1: Numerically integrated planetary growth tracks evolving according to 2D Hill-accretion (Eq 2.27) up until reaching M_{iso} at which point further growth is due to gas accretion (Eq 2.31). All protoplanets are initiated with $M = 0.01\ M_{\text{E}}$ and are subject to migration following the modified Type-1 migration rate (Eq 2.36). The growth tracks in the upper plot are initiated at $t_0 = 0.7$ Myr while the growth tracks in the lower plot are initiated at $t_0 = 1.2$ Myr. M_{iso} is shown as a function of r for two values of α_{v} corresponding to the two different α values used for the growth tracks in both the upper and lower plot.

to it being proportional to M^4. Protoplanets that reach M_{iso} with too low a mass therefore never manage to accrete the mass needed for the migration rate to slow down. This is clearly demonstrated by the growth track initiated at $r_0 = 10$ AU and $t_0 = 0.7$ Myr in a protoplanetary disk with $\alpha = \text{St} = \xi = 0.01$ which manages to reach M_{iso} without ever turning vertical. The fact that the growth track initiated with the same α/St, ξ and r_0 does turn vertical when initiated at the later starting time is due to $\dot{M}_{\text{g}}$ decreasing over

time. From Eq 2.1 one notes that this decrease leads to an decrease in Σ_g and thus serves to lower the migration rate.

Table 4.1: Final masses and radial positions of planets initiated at $r_0 = 30$ AU and $t_0 = 0.7$ Myr when using the Runge-Kutta method as well as when using the Euler method

		Runge-Kutta		Euler	
α/St	ξ	M [M_E]	r [AU]	M [M_E]	r [AU]
0.01	0.01	1478.2	2.0153	1459.6	1.9976
	0.02	2468.3	2.8666	2464.1	2.8388
0.02	0.01	465.39	4.5348	445.23	4.5258
	0.02	1892.7	4.4989	1883.4	4.4652

By decreasing the value used for α in the simulations a lower u_r is obtained and as $\dot{M}_g$ is set there must be an increase in Σ_g as a response. Similarly, as v_r is proportional to u_r there will also be a corresponding increase in Σ_p. As a consequence of these increases to the surface densities, the protoplanet migration rate and core growth rate will both increase as can be seen from Eq 2.27 and 2.32. However, the increase in the migration rate is greater than the increase in the growth rate. This happens as even though Σ_g and Σ_p are both proportional to $1/\alpha$ the growth rate is also proportional to $\mathrm{St}^{2/3}$ and St is set to be equal to α in all simulations. Thus the growth rate is ultimately proportional to $1/\alpha^{1/3}$. As such, for a given value of ξ the tracks produced in the disk with $\alpha = 0.01$ begin to turn horizontal at a lower mass than those produced in the disk with $\alpha = 0.02$ as can be seen in figure 4.1.

Also of note is that two of the growth tracks which were initiated at $r_0 = 30$ AU and $t_0 = 1.2$ Myr never manage to accrete enough mass to reach M_{iso} before the dissipation of the protoplanetary disk. This is in part due to the late starting time of the protoplanets represented by these growth tracks. However, it is also caused by the protoplanets evolving in a protoplanetary disk with a low value for ξ which lowers the core growth rate. Of these two growth tracks one manages to both accrete more mass and migrate a greater distance than the other. This difference is a result of the tracks evolving according to separate α/St values which, as detailed above, impacts both the core growth rate and the migration rate.

From table 4.1 one notes that there is a noticeable difference in the results when using the Runge-Kutta method and the Euler method. This difference is quite small however with the greatest difference occurring for the final mass of planets initiated with $\alpha/\mathrm{St} = 0.02$ and $\xi = 0.01$ being less than 5 percent regardless of which order the ratio of the masses is taken.

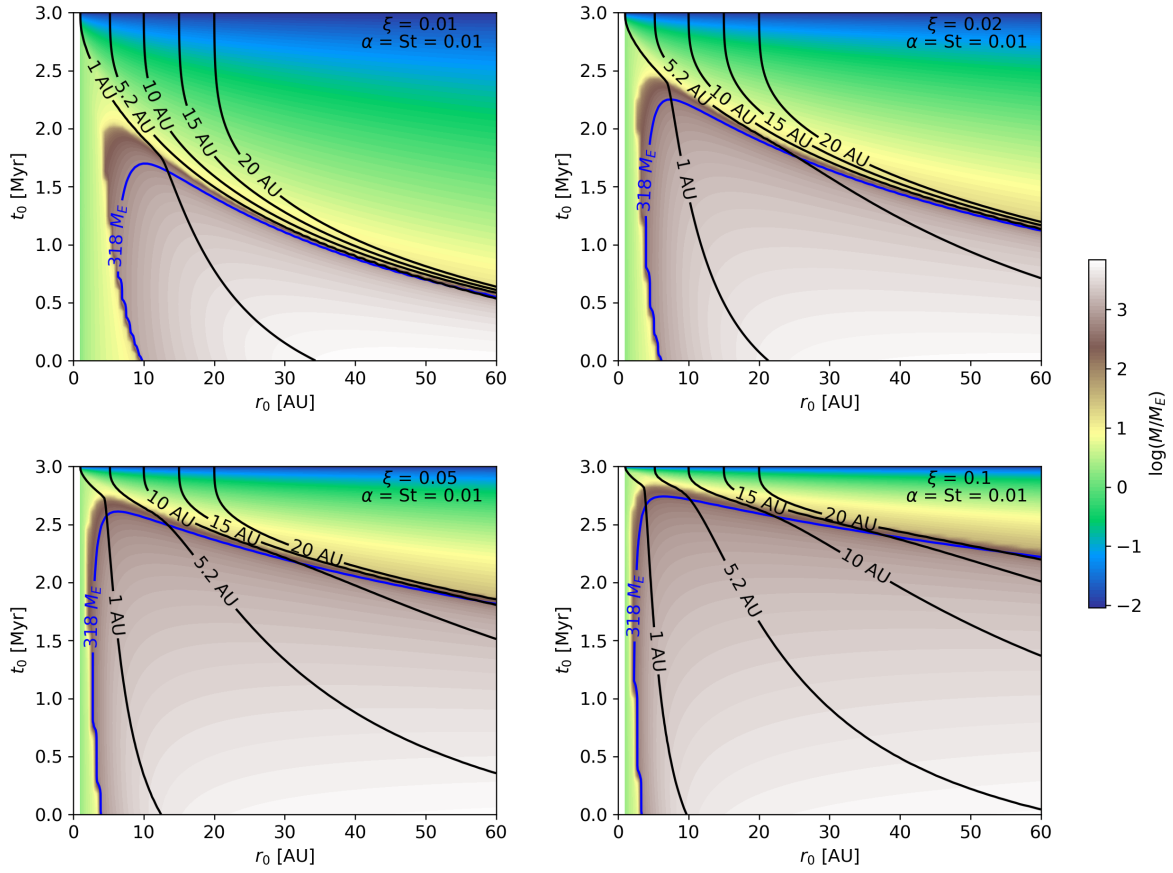

Figure 4.2: Growth maps showing the final masses (color graded contours) and final positions (black contours) of protoplanets growing and migrating in protoplanetary disks with $\alpha = \mathrm{St} = 0.01$ and four separate values for ξ. The color contours have been normalized by M_E. The mass contour of the Jupiter mass (318 M_E) has been highlighted with a blue contour to make the intersection between it and the Jupiter position contour (5.2 AU) easy to pick out.

4.2 Growth maps

Figure 4.2 presents growth maps used to determine r_0 and t_0 for possible Jupiter analogues. In the figure four separate growth maps are displayed, each one of which is the product of simulations in protoplanetary disks with different values for ξ. All four growth maps are, however, produced using the same value for α/St. Growth maps which are the product of simulations in protoplanetary disks with the same four ξ values as figure 4.2 but a different α/St value are presented in figure 4.3. The final masses of the simulated protoplanets are represented by color graded contours in the figures. Due to there being some difficulty in

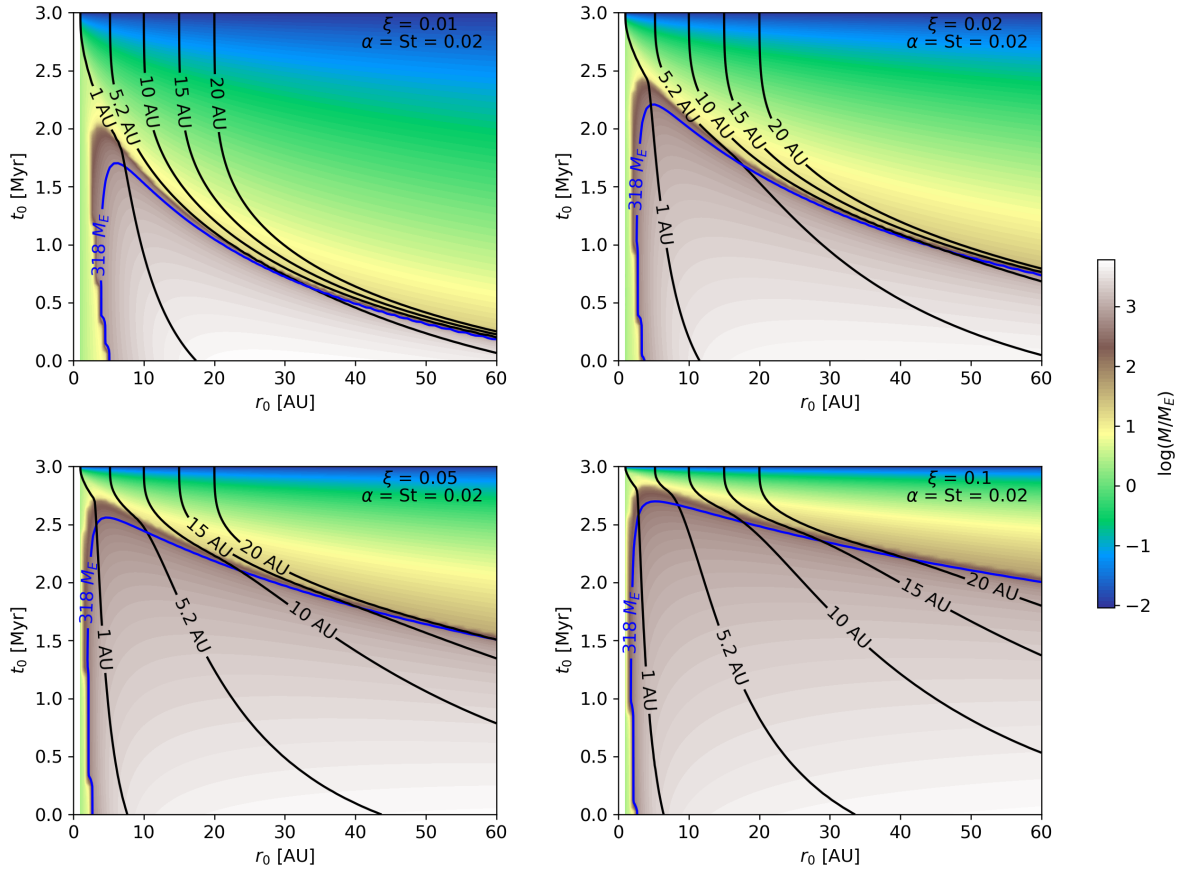

Figure 4.3: Growth maps showing the final masses (color graded contours) and final positions (black contours) of protoplanets growing and migrating in protoplanetary disks with $\alpha = \mathrm{St} = 0.02$ and four separate values for ξ. As for figure 4.2 the color contours have been normalized by M_E and the mass contour of the Jupiter mass (318 M_E) has been highlighted with a blue contour.

determining the exact shade of a certain mass the contour following the Jupiter mass of 318 M_E has been highlighted with a solid blue contour in all eight growth maps.

Jupiter analogues are indicated in the growth maps by the intersections between the Jupiter mass contours and the Jupiter position contours. The coordinates of these intersections and thus the starting times and initial positions of the Jupiter analogues, which have been extracted using the `Python` module `shapely`, are presented in table 4.2 along with distance d over which they have migrated.

As can be seen from the growth maps and the values of table 4.2, the intersections between the Jupiter mass contours and the Jupiter position contours are pushed towards earlier starting times and initial distances farther from the host star as ξ is decreased (so too are,

of course, the starting times and positions of all simulated protoplanets). The change in both the starting time and position stems from the fact that by lowering ξ the core growth rate is reduced as was mentioned for the growth tracks. Needless to say, this reduction of the core growth rate means that it takes more time to accrete a core with a given mass as compared to when using a higher value for ξ. However, as the protoplanets spend more time accreting their core due the reduced growth rate they also spend more time with a mass much lower than M_{gap}. Thus said protoplanets will migrate in the fast migrating region around 1-10 M_{E} where the growth tracks follow a nearly horizontal path over a greater period of time. Thereby resulting in an increased migration distance to produce a protoplanet of a given mass.

Table 4.2: Starting times and initial positions of Jupiter analogues growing and migrating in protoplanetary disks with $\alpha = \text{St} = 0.01$ and $\alpha = \text{St} = 0.02$ as well as four separate values for ξ. The data has been extracted from the data used to produce the growth maps of figures 4.2 and 4.3.

α/St	ξ	r_0 [AU]	t_0 [Myr]	d [AU]
0.01	0.01	53.29	0.64	48.09
	0.02	25.44	1.75	20.24
	0.05	13.46	2.49	8.26
	0.1	10.25	2.71	5.05
0.02	0.01	33.39	0.64	28.19
	0.02	17.67	1.68	12.47
	0.05	10.47	2.43	5.27
	0.1	8.47	2.67	3.27

By increasing the value of α/St a push is instead seen towards shorter migration distances for a given value of ξ as this decreases not only the core growth rate but the migration rate as well. The change in starting time due to this increase on the other hand is in the same direction as when increasing ξ. This change is, however, minor compared to the change in initial distance. This is in part due to the changes in α/St having a smaller impact on the growth rate than the migration rate. It is also due, in part, to the impact on the starting time that comes with a change in the growth rate being counteracted by the change in migration distance before reaching M_{iso} that comes with an initial distance closer to the host star. This change in migration distance affects the time as it takes for a planet to begin gas accretion and as such affects the starting time.

As a result of the increased migration distance that comes from using a protoplanetary disk with a low value for ξ there is an accompanying increase in the production of hot Jupiters with final positions interior to 1 AU. On the other hand, high values for ξ will increase the production of giant planets in general due to the accompanying increase in the growth rate. Both of these phenomena become evident when comparing the growth maps. This comparison also shows how the decrease in the growth and migration rates

that comes from increasing the value of α/St in the simulations mitigates the production of both these types of planets over all.

Another point to note about the growth maps, though it might seem obvious, is that the protoplanets grow ever closer to forming in situ as they begin their accretion in later stages of the disk lifetime. This happens simply due to the fact that the protoplanets have an ever decreasing time to migrate. The path of the position contours towards near in situ formation is, however, heavily influenced by the value of the ξ parameter as detailed above.

Chapter 5

Discussion & conclusions

The first point that I believe should be made here is regarding the reliability of the results as several assumptions and simplifications have been made in the simulations. Foremost of these are the facts that 3D Hill-accretion is not taken into account and that the protoplanets are assumed to evolve without being influenced by the simultaneous formation of other planetesimals and protoplanets.

The impact of the simplification that is ignoring 3D accretion becomes clearly visible when comparing the results of this thesis with the results of Johansen et al. (2018) where 3D accretion is implemented in the simulation of growth maps. The growth maps of said paper makes a good comparison as the planets they represent evolve following the same equations used in this thesis aside from 3D accretion being implemented. Thus the protoplanetary disk parameters used to generate the growth maps of figure 4.2 in this thesis were specifically chosen to match those of Johansen et al. (2018) so that a comparison could be made. From this comparison one notes that planets grow more massive in general when 3D accretion is not taken into account. Thus one can deduce that accretion is generally more effective in the 2D accretion regime than in the 3D accretion regime without making a detailed comparison of Eq 2.26 and Eq 2.27. Also of note is the distance over which the forming planets migrate in the two cases. There is a noticeable difference as the time it takes to accrete the core is effected by the inclusion of 3D accretion in the simulations.

I cannot speak as much to the impact on the results due to protoplanets forming without being influenced by the simultaneous formation of other planetesimals and protoplanets. However, it is safe to say that there is an impact. This becomes most obvious when considering the effects of the annular gap created by massive cores. As the pressure bump created by such gap halts the flow of pebbles any core that is undergoing pebble accretion and is forming interior to the gap will have its growth stunted.

Putting the deficiencies of the simulations aside. I find, as can be seen from table 4.2, that a planet which ultimately ends up with the mass and orbit of Jupiter undergoes several tens of AU of migration when forming in a protoplanetary disk with the lowest values of

ξ used in the thesis. This is true both in the case $\alpha = \mathrm{St} = 0.01$ and $\alpha = \mathrm{St} = 0.02$ though the difference between the two cases is significant. The migration distance quickly drops as ξ is increased on the other hand and is reduced to below 10 AU for the highest values of ξ used. However, from the table one notes that the influence of changes in ξ on the migration distance drops quickly as the value of ξ increases. As does the difference between using $\alpha = \mathrm{St} = 0.01$ and $\alpha = \mathrm{St} = 0.02$, with the difference in migration distance changing from just over 20 AU in the case of $\xi = 0.01$ to less than 2 AU in the case of $\xi = 0.1$.

There are still some issues with the smoothness of the contours even when using the smaller time step of 3.2 instead of 3.1. Whether this is simply due to the time step being to large I cannot not say with any certainty, though the decrease from 3.1 to 3.2 did have an impact on the smoothness of the contours. Nor can I speak to why this unevenness is only present on some parts of some contours and only for certain protoplanetary disk parameters, I can only note that it is present to make the reader aware of this flaw. As one will not from table 4.1 this might have been alleviated by using the Runge-Kutta method when producing the growth maps. However, the Runge-Kutta method is computation heavy and each growth maps contains the final masses and positions of ten thousand planets. As such I did not have the processing power necessary to finish the simulations in a timely manner when using this more accurate method.

It should also be mentioned that the `Python` module `shapely` was utilized without full comprehension of how it manipulates the provided the data in order to correctly determine the intersection coordinates of two contours. Therefore the accuracy of the results produced by the module were cross checked (and found to be accurate) several times. This was done using intersecting contours produced on interactive plots where the intersection could simply be zoomed in on until the coordinates could be read of the plot with a desired accuracy.

Bibliography

Bai, X.-N. & Stone, J. M. 2013, ApJ, 769, 76

Birnstiel, T., Ormel, C. W., & Dullemond, C. P. 2011, A&A, 525, A11

Bitsch, B., Johansen, A., Lambrechts, M., & Morbidelli, A. 2015, A&A, 575, A28

Bitsch, B., Morbidelli, A., Johansen, A., et al. 2018, A&A, 612, A30

Chambers, J. E. 2009, Annual Review of Earth and Planetary Sciences, 37, 321

D'Angelo, G. & Lubow, S. H. 2010, ApJ, 724, 730

Hartmann, L., Calvet, N., Gullbring, E., & D'Alessio, P. 1998, ApJ, 495, 385

Hayashi, C. 1981, Progress of Theoretical Physics Supplement, 70, 35

Ikoma, M., Nakazawa, K., & Emori, H. 2000, ApJ, 537, 1013

Johansen, A., Blum, J., Tanaka, H., et al. 2014, Protostars and Planets VI, 547

Johansen, A., Ida, S., & Brasser, R. 2018, arXiv e-prints

Johansen, A. & Lambrechts, M. 2017, Annual Review of Earth and Planetary Sciences, 45, 359

Kanagawa, K. D., Tanaka, H., & Szuszkiewicz, E. 2018, ApJ, 861, 140

Lambrechts, M. & Johansen, A. 2014, A&A, 572, A107

Lambrechts, M., Johansen, A., & Morbidelli, A. 2014, A&A, 572, A35

Lin, D. N. C., Bodenheimer, P., & Richardson, D. C. 1996, Nature, 380, 606

Mayor, M. & Queloz, D. 1995, Nature, 378, 355

Nelson, R. P. 2018, Planetary Migration in Protoplanetary Disks, 139

Ormel, C. W. & Klahr, H. H. 2010, A&A, 520, A43

Ros, K. & Johansen, A. 2013, in AAS/Division for Planetary Sciences Meeting Abstracts, Vol. 45, AAS/Division for Planetary Sciences Meeting Abstracts #45, 510.03

Simon, J. B., Armitage, P. J., Li, R., & Youdin, A. N. 2016, ApJ, 822, 55

Zsom, A., Ormel, C. W., Güttler, C., Blum, J., & Dullemond, C. P. 2010, A&A, 513, A57

Appendix A

Github-repository

For the full code developed for the thesis see `https://github.com/Calle-Ahlgren/Bachelors-Thesis-Collected-Code`. The code is only lightly commented, it is however simple enough to be understood in tandem with the thesis assuming the reader possesses a beginner-level understanding of `Python`-programming.